■ **Materials Science inc. Nanomaterials & Polymers**

Facile Synthesis of a NiCo$_2$O$_4$ Nanoparticles Mesoporous Carbon Composite as Electrode Materials for Supercapacitor

Nghia V. Nguyen,[a, b] Thu V. Tran,[c] Son T. Luong,[c] Thao M. Pham,[c] Ky V. Nguyen,[c] Thao D. Vu,[c] Hieu S. Nguyen,[d] and Nguyen V. To*[e, f]

Combination the materials together is a direct and forceful strategy to improve the electrochemical properties of each raw material. Herein, we present the method of hydrothermal process and treatment/calcination combination that is easy to synthesize a NiCo$_2$O$_4$ nanoparticles-mesoporous carbon composite (C/NiCo$_2$O$_4$). The result study electrochemical properties of materials revealed that the C/NiCo2O4 composite has excellent electrochemical properties compare with pristine NiCo$_2$O$_4$ or carbon. In particular, maximum specific capacitance of C/NiCo$_2$O$_4$ material at a current density of 1 A.g^{-1} is 204.28 F.g^{-1}, meanwhile the C$_s$ of carbon and NiCo$_2$O$_4$ are 25.06 F.g^{-1} and 178.78 F.g^{-1}, respectively. In addition, C/NiCo$_2$O$_4$ material also showed excellent capacitance retention, C$_s$ maintained to 90.35% after 3000 charge-discharge continuous cycles. The results show that the C/NiCo$_2$O$_4$ is a promising material for application as supercapacitor electrode.

1. Introduction

Today, global fossil fuel reserves are running out, the world population is growing meanwhile, the demand of energy storage devices is increasing.[1] This creates a great motivation to promote research and development of clean and friendly energy storage devices. In recent years, supercapacitor (SCs) is known as a promising energy storage device because it has many advantages, such as: high energy, superior energy density, excellent durability and high efficiency.[2]

Based on to the charging mechanism, SCs are divided into two main categories: electrical double-layer capacitors (EDLCs) and Faradaic redox reaction pseudo-capacitors (PCs).[2a,3] EDLCs accumulate electrical energy based solely on process absorption/desorption of electrolyte ions at the interface of electrolytes and electrodes. Therefore, carbon base materials with large specific surface area are commonly used for EDCLs, such as activated carbon,[4] carbon foam,[5] carbon nanotubes,[6] graphene.[7] PCs operate based on redox reactions between active material and ions of electrolyte on interface of their, so their working processes are limited by kinetics of redox reaction. Compared with EDLCs, PCs provide higher energy density, but lower power density. The well-known electrode materials for PCs are substances that have multiple oxidation states such as nano-structured metal oxides (MnO$_2$, NiCo$_2$O$_4$),[8] metal sulfides,[9] conductive polymers (PPy, PEDOT, PANI).[10]

Recently, transition metal oxides have received intensive attention as electrode materials for energy storage applications because of their high specific capacitance (Cs), natural abundance, and easy fabrication to obtain nanostructures.[11] Among them, NiCo$_2$O$_4$ oxide is a promising candidate for the applications because it consists of multiple oxidation state metals, has high electrical conductivity and superb capacity storage.[8c] In addition, NiCo$_2$O$_4$ hybrid metal oxides possess higher conductivity and capacity than both NiO and Co$_3$O$_4$.[8b,12] However, most transition metal oxides have certain limitations: low power density, poor rate capability and cycling stability.[13] The number of studies has been investigated to resolve the problems and mainly focused on the direction of combining transition metal oxides with different conductive materials, especially carbon-based materials.[14] Carbon is chosen because it has outstanding features such as superior electrical conductivity, high energy density, excellent capacitance retention and natural abundance.[15] For example, Vediyappan Veeramani et al. successfully synthesized porous carbon nanosheets decorated NiCo$_2$O$_4$ with 3,4-ethylenedioxythiophene polymers (EDOT) in the form of carbon sources (C@NiCo$_2$O$_4$), the results show that when tested in the same conditions, Cs of C@NiCo$_2$O$_4$ was 162% higher than the C$_s$ of NiCo$_2$O$_4$.[16] Similarly,

[a] *Dr. N. V. Nguyen*
Research Center of Advanced Materials and Applications, Institute of Architecture, Construction, Urban and Technology, Hanoi Architectural University, Hanoi 100000, Vietnam.

[b] *Dr. N. V. Nguyen*
Department of Physics, Open Training Institute, Hanoi Architectural University, Hanoi 100000, Vietnam.

[c] *Dr. T. V. Tran, S. T. Luong, Dr. T. M. Pham, K. V. Nguyen, Dr. T. D. Vu*
Department of Chemical Engineering, Le Quy Don Technical University, 236 Hoang Quoc Viet, Ha noi 100000, Vietnam.

[d] *Dr. H. S. Nguyen*
Institute of Materials Science, VAST, 18 Hoang Quoc Viet, Hanoi 100000, Vietnam

[e] *N. V. To*
Institute of Research and Development, Duy Tan University, Danang 550000, Vietnam
E-mail: tovannguyen@duytan.edu.vn

[f] *N. V. To*
The Faculty of Environmental and Chemical Engineering, Duy Tan University, Danang 550000, Vietnam.

Supporting information for this article is available on the WWW under https://doi.org/10.1002/slct.202001410

ChemistrySelect

Full Papers
doi.org/10.1002/slct.202001410

Chemistry Europe
European Chemical
Societies Publishing

involving the combination of $NiCo_2O_4$ and carbon based materials: $rGO@NiCo_2O_4$,[17] $rGO@NiCo_2O_4$ on nickel foam,[18] $rGO@MnFe_2O_4@PPy$,[19] core-shell of carbon nanosphere and $NiCo_2O_4$,[20] these studies revealed that composite materials have C_s outperformed to its individual materials. However, the fabrication methods are complicated, high cost, not environment-friendly, and difficult to implement in large scale, which limit the practical applications as supercapacitor electrodes.

In this work, we provide a simply and eco-friendly method for synthesizing $C/NiCo_2O_4$ composite with high electrochemical efficiency. Where, carbon source is a popular commercial product and only one step calcination to obtain carbon without further processing. The results showed that, $C/NiCo_2O_4$ composite was successfully synthesized and the $NiCo_2O_4$ nanoparticles are evenly distributed on the carbon porous. The combination of carbon and $NiCo_2O_4$ creates a new material that operates under a hybrid capacitor mechanism. The material has higher electrochemical effective compare to the individual $NiCo_2O_4$ or carbon. In particular, the long-cycled test results indicated that $C/NiCo_2O_4$ material is capable of maintaining excellent capacitance.

2. Results and Discussion

2.1. Structural and morphological characterization

The XRD profile observed for $NiCo_2O_4$ and $C/NiCo_2O_4$ are show in Figure 1a. The main diffraction peaks in XRD pattern of $NiCo_2Co_4$ material located at 19.01, 31.22, 36.73, 38.35, 44.67, 55.52, 59.14 and 65.02° are indexed to the (111), (220), (311), (222), (400), (422), (511) and (440) planes, respectively and can be assigned to $NiCo_2O_4$ phase (JCPDS #73-1702), which has cubic spinel structure and space group Fd-3 m (227). The XRD pattern of $C/NiCo_2O_4$ material also shown all diffraction peaks of $NiCo_2O_4$ phase but with weaker diffraction intensity. It has been known that the XRD peak intensity is related to both the crystal structure and composition. Therefore, the reduction in the intensity of XRD pattern of $C/NiCo_2O_4$ as compared to $NiCo_2O_4$ material is thought to be due to their difference in composition. In addition, there are no diffraction peaks of carbon in XRD pattern of the $C/NiCo_2O_4$ composite indicating that carbon in the composite is amorphous. In all XRD profile unable to detect other peaks indicates that the $C/NiCo_2O_4$ composite has a high purity.

Figure 1 **b** shows TG curves of carbon, $NiCo_2O_4$ and $C/NiCo_2O_4$. It can be seen in all TGA curves, there is a small mass loss due to evaporation of moisture. For TGA curve of carbon, the mass loss in the temperature range from 400 to 600 °C is
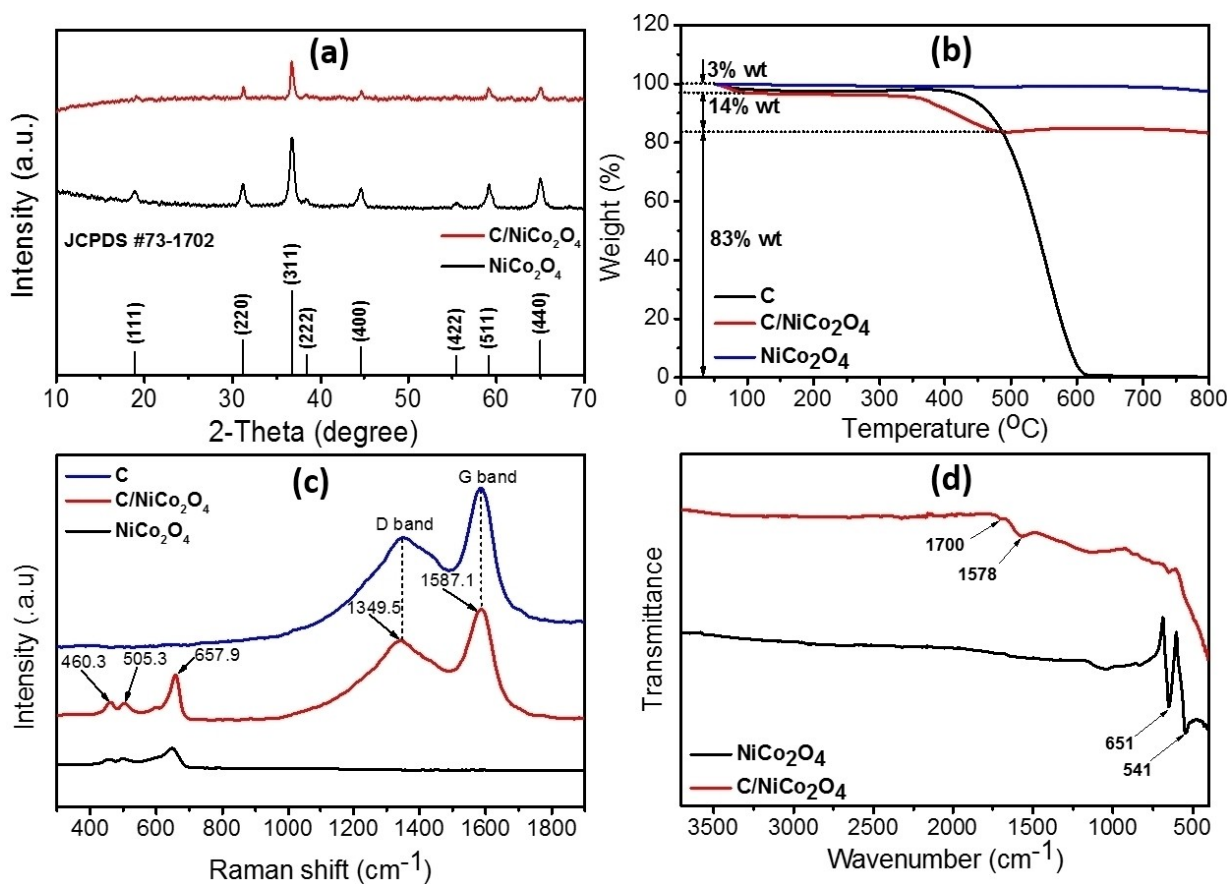

Figure 1. (a) XRD patterns of the $NiCo_2O_4$ and $C/NiCo_2O_4$; **(b)** TG analysis of Carbon, $NiCo_2O_4$ and $C/NiCo_2O_4$; **(c)** Raman spectra of Carbon, $NiCo_2O_4$ and $C/NiCo_2O_4$; **(d)** FT-IR of $NiCo_2O_4$ and $C/NiCo_2O_4$.

ChemistrySelect

Full Papers
doi.org/10.1002/slct.202001410

**Chemistry
Europe**
European Chemical
Societies Publishing

attributed to the combustion of amorphous carbon; when the temperature is higher than 600 °C, the weight of analytical sample is approximately of zero, this result indicates that there are no inorganic impurities. Meanwhile, the burning of amorphous carbon in $C/NiCo_2O_4$ sample at temperature range from 350 to 500 °C shows the mass of analysed sample decreased by 12.4%, which indicates that the ratio of carbon in the $C/NiCo_2O_4$ composite is ~ 12.4%. It also reveals that the presence of $NiCo_2O_4$ in $C/NiCo_2O_4$ lead to carbon burned at lower temperature, which has been reported in other hybrid materials such as $rGO@MnFe_2O_4@PPy$,[19] carbon fiber/Ni–Co composites.[21]

The Raman spectra of $NiCo_2O_4$, Carbon and $C/NiCo_2O_4$ samples shown in Figure 1c. In the Raman spectrum of carbon showed the presence of double peaks at 1349.5 and 1587.1 cm^{-1}, which can be assigned to the D band and G band of carbon amorphous, respectively.[22] These observations are also evident in the Raman spectrum of $C/NiCo_2O_4$ and indicated the presence of carbon amorphous in the $C/NiCo_2O_4$ material. In addition, the appearance of peaks at 460.3, 505.3 and 657.9 cm^{-1} in the Raman spectrum of $C/NiCo_2O_4$ attributed to the E_g, F_{2g}, and A_{1g} vibration modes of the $NiCo_2O_4$ spinel structure, respectively.[23] This the result match well with the Raman spectrum of $NiCo_2O_4$ and confirm the formation of $NiCo_2O_4$ in the synthesized materials.

Figure 1d presents the FT-IR spectra of all synthesized materials. In the spectrum of $NiCo_2O_4$ material, there are two sharp peaks at low frequencies (541 cm^{-1} and 651 cm^{-1}), which correspond to the stretching vibrations of Ni—O and Co—O bonds in $NiCo_2O_4$.[24] Meanwhile, two peaks corresponding to Ni—O and Co—O bonds in the FT-IR of $C/NiCo_2O_4$ composite appearance with weak intensity, this due to the existence of carbon in its. In addition, the presence of two peaks at roughly 1578 and 1700 cm^{-1} can be assigned to the stretching vibrations of the C—C and C=O bonds, respectively.[24–25] The results proved the presence of carbon in the $C/NiCo_2O_4$ material.

The morphology of carbon, $NiCo_2O_4$ and $C/NiCo_2O_4$ were investigated using SEM, TEM measurements and the result showed in Figure 2. As shown in SEM and TEM images, $NiCo_2O_4$ particle has a polyhedral shape with some degrees of aggregation and its average size is typically about 50 nm. Meanwhile, SEM and TEM images of $C/NiCo_2O_4$ show that the $NiCo_2O_4$ particles are uniformly distributed into amorphous
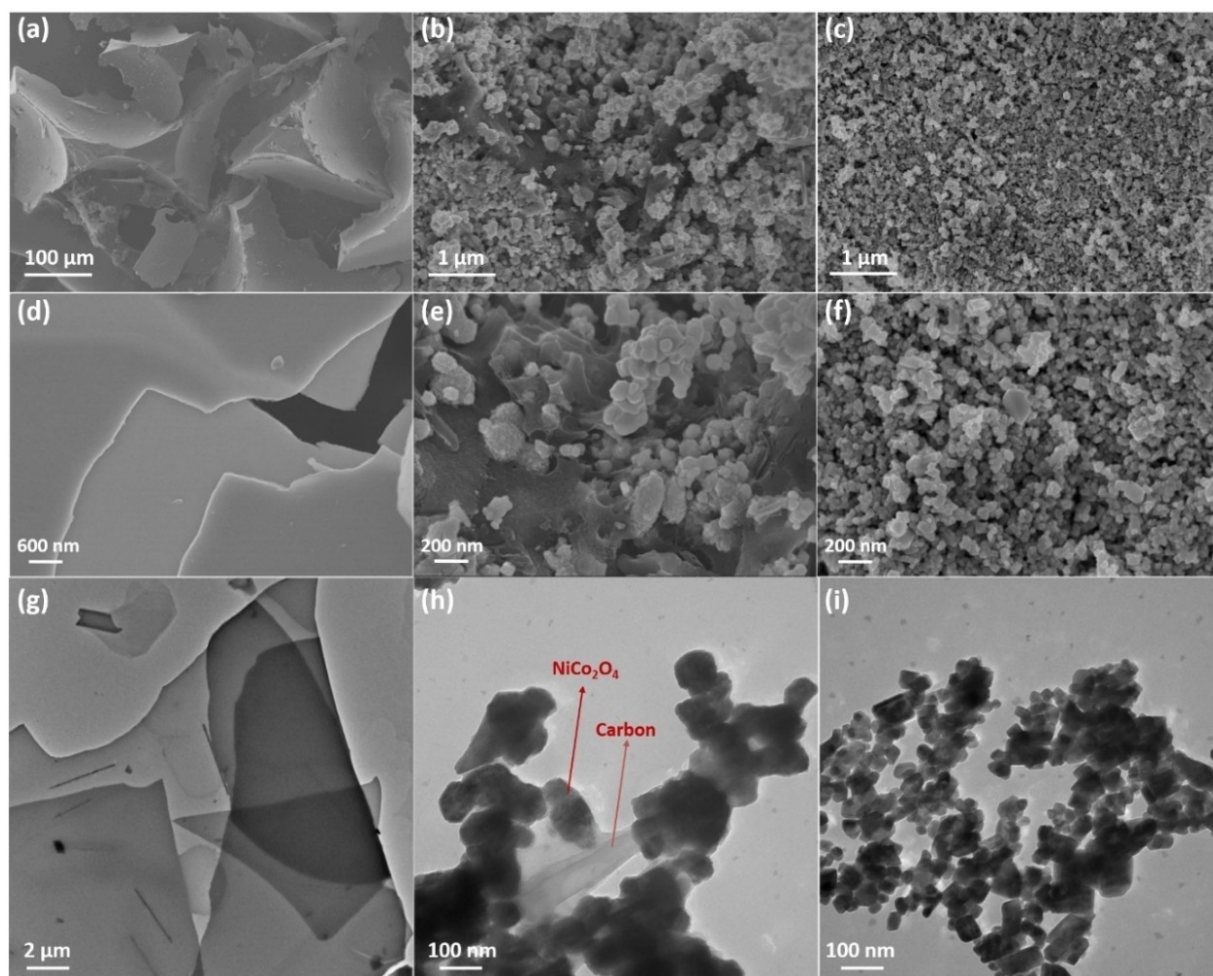
Figure 2. SEM and TEM images of Carbon (a, d, g); $C/NiCo_2O_4$ (b, e, h) and $NiCo_2O_4$ (c, f, i)

carbon and its average size is about 100 nm, suggesting that $NiCo_2O_4$ precursors added into molten sucrose result in a larger $NiCo_2O_4$ agglomeration but keep its polyhedron shape not changed. The SEM, TEM images of carbon show that the morphology of amorphous carbon is like muddy clays and the surface of the carbon is clean. The additional SEM images of the materials can be seen in the Supporting Information [**Supporting Figure S1, S2, and S3**].

To evaluate chemical composition of materials, we were using energy dispersive X-ray spectroscopy (EDS) analysis and the result showed in Figure 3. The EDS results confirm the presence of C and O in carbon; Ni, Co, and O in $NiCo_2O_4$; C, Ni, Co, and O in $C/NiCo_2O_4$. The present of oxygen atomic in the carbon sample with atomic percentage about 13.51%, which indicates that 1 hour carbonization is not long enough, therefore need to consider more the effect of carbonization time or temperature to properties of carbon obtained. Figure 3f shows the EDS result of $NiCo_2O_4$ material, where the atomic ratio of Ni/Co/O is 1: 2.1: 4.1 indicating that the component of the $NiCo_2O_4$ product is closed to the desired $NiCo_2O_4$ phase. Meanwhile, atomic ratio of Ni/Co/O in the $C/NiCo_2O_4$ composite (Figure 3e) is 1:2.18:5.39 [**Supporting Table S1**]. The ratio of Ni/Co in the $NiCo_2O_4$ and $C/NiCo_2O_4$ is equivalent but atomic ratio of Ni/O change from 1:4.1 up to 1:5.39. As shown in the EDS results for carbon materials (Figure 3d), O atom appear in carbon materials with a percentage of about 13.5%. Due to the total of O atoms in the $C/NiCo_2O_4$ material include of O in carbon and O in $NiCo_2O_4$, the percentage of O atoms in $C/NiCo_2O_4$ is evidently higher than that of $NiCo_2O_4$.

2.2. Electrochemical characteristics *CV analysis*

To estimate electrochemical performance of synthesized materials, CV test was performed at a scan rate of 20 mV.s^{-1} for all materials and the result showed in Figure 4a. The CV curve of carbon looks like a rectangle, which shows the working process of carbon complying with the EDLC mechanism.[7] Meanwhile, in CV curves of $C/NiCo_2O_4$ and $NiCo_2O_4$, a pair of redox peaks is clearly observed, which were attributed to redox reactions relating to conversions of A-O/A-O-OH (A=Ni or Co).[26] In a potential window of 0 to 0.5 V in an alkaline solution, redox reaction between $NiCo_2O_4$ and OH^- ion of KOH electrolyte can be described by the following equations:

$$NiCo_2O_4 + OH^- + H_2O \;\; NiOOH + 2CoOOH + e^- \qquad (1)$$

$$CoOOH + OH^- \;\; CoO_2 + H_2O + e- \qquad (2)$$
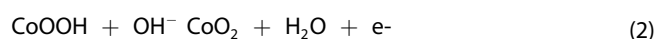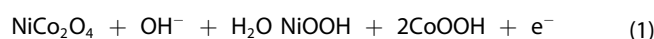
The results confirming that, $C/NiCo_2O_4$ and $NiCo_2O_4$ exhibit pseudocapacitor behaviour based on electron transfer process, and their main mechanism for energy storage is based on redox reactions. Figure 4a also shows that the CV curve of $C/NiCo_2O_4$ has internal area higher than carbon and $NiCo_2O_4$, indicating that $C/NiCo_2O_4$ has the largest C_s. The Cs improvement of the $C/NiCo_2O_4$ material compared pristine carbon or $NiCo_2O_4$ is ascribed to a synergistic effect of carbon and $NiCo_2O_4$ components in its.[17,19, 21]

CV measurements of $C/NiCo_2O_4$ material conducted at different scan rates from 10–100 mV.s^{-1} within the potential range of −0.45 - 0.45 V is displayed in Figure 4b. The increasing of current densities at redox peak when increasing scan rate indicate that the redox reactions on surface of $C/NiCo_2O_4$ electrode occur rapidly,[27] which is essential for being super-
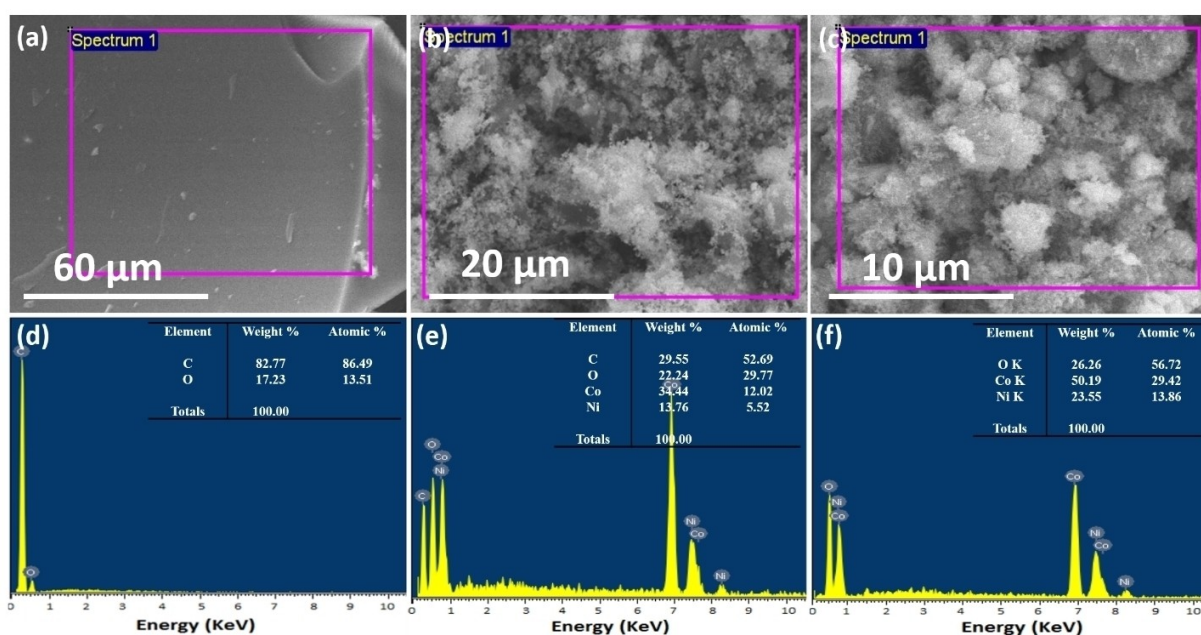

Figure 3. SEM images and corresponding EDS profiles of Carbon (**a, d**); $C/NiCo_2O_4$ (**b, e**) and $NiCo_2O_4$ (**c, f**).

ChemistrySelect

Full Papers
doi.org/10.1002/slct.202001410

**Chemistry
Europe**
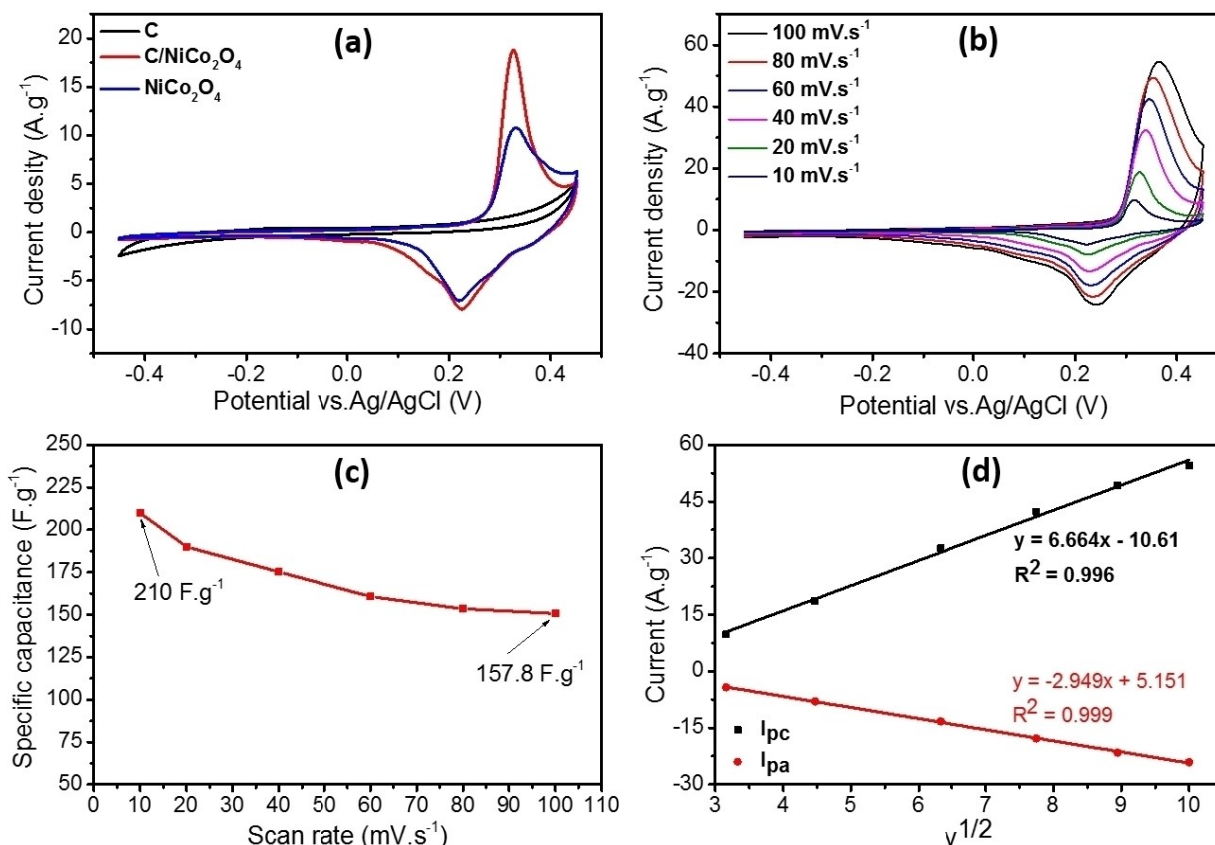European Chemical
Societies Publishing

Figure 4. (a) CV curves of all materials at a scan rate of 20 mV.s^{-1}; (b) CV curves of C/NiCo$_2$O$_4$ at different scan rates; (c) C$_s$ of C/NiCo$_2$O$_4$ at different scan rates; (d) Randles-Sevcik plots for C/NiCo$_2$O$_4$.

capacitor electrode materials. Figure 4c displays the C$_s$ of C/NiCo$_2$O$_4$ materials at different scan rate. As shown in Figure 4c, the C$_s$ of the C/NiCo$_2$O$_4$ increases as scanning rate decreases: when increases scan rates from 10–100 mV.s^{-1}, C$_s$ of C/NiCo$_2$O$_4$ decreases from 210–157.8 F.g^{-1}. The small decreases of C$_s$ when increases scan rate suggest C/NiCo$_2$O$_4$ has high rate capacity, which reflects its charging performance at a high charging rate. In scan rate range, rate capacity is the ratio between the C$_s$ at maximum scan rate and the C$_s$ at minimum scan rate. The rate capacity of the C/NiCo$_2$O$_4$ is 0.75, this value is superior proving that C/NiCo$_2$O$_4$ material not only capably delivers high energy density but also high power density. More specifically, both the anodic peak current (I$_{pa}$) and the cathodic peak current (I$_{pc}$) increase linearly with the square root of the scan rate ($\nu^{1/2}$) (Figure 4d), which consisted well with the Randles-Sevcik equation.[28] These observations suggest that redox reactions occurred at the electrode/electrolyte interface are apparently reversible and only limited by electrolyte diffusion.

GCD analysis

To evaluate the Cs of all synthesized materials, GCD measurements were conducted within the potential range of −0.45 to 0.45 V at different current densities from 1 to 6 A g^{-1} and the

GCD voltage profile of all materials showed in Figure 5(**a–c**). The GCD curve of carbon is almost triangular, indicating that the electrical storage mechanism is EDLC. The result is completely consistent with the CV curve of the carbon in Figure 4a. The GCD voltage profiles of C/NiCo$_2$O$_4$ and NiCo$_2$O$_4$ (Figure 5b and **5c**) show one voltage plateau, which match well with the I$_{pc}$ and I$_{pa}$ peaks occurred in CV curves (Figure 4a), indicating that the NiCo$_2$O$_4$ and C/NiCo$_2$O$_4$ exhibit pseudocapacitor behaviour based on electron transfer process and their primary energy storage mechanism is based on redox reactions. The small difference between discharge and charge potential plateau in GCD profiles indicates a high electrochemical reversibility and small series resistances of the electrode.[26,28]

As analyzed in the part result of CV measurement, rate capability is an important parameter for materials use as supercapacitor electrode. To estimate rate capability, the C$_s$ of all materials at different current densities were calculated from GCD profiles and plotted in Figure 5d, the C$_s$ of all materials were listed in the Supporting Information [**Supporting Table S2**]. It can be seen that, the small decreases of C$_s$ for all materials when discharge current density increases showing the fast Faradaic redox reaction kinetics and the remarkable rate capability of the electrode materials. At the same current density, C$_s$ of C/NiCo$_2$O$_4$ composite material is always higher
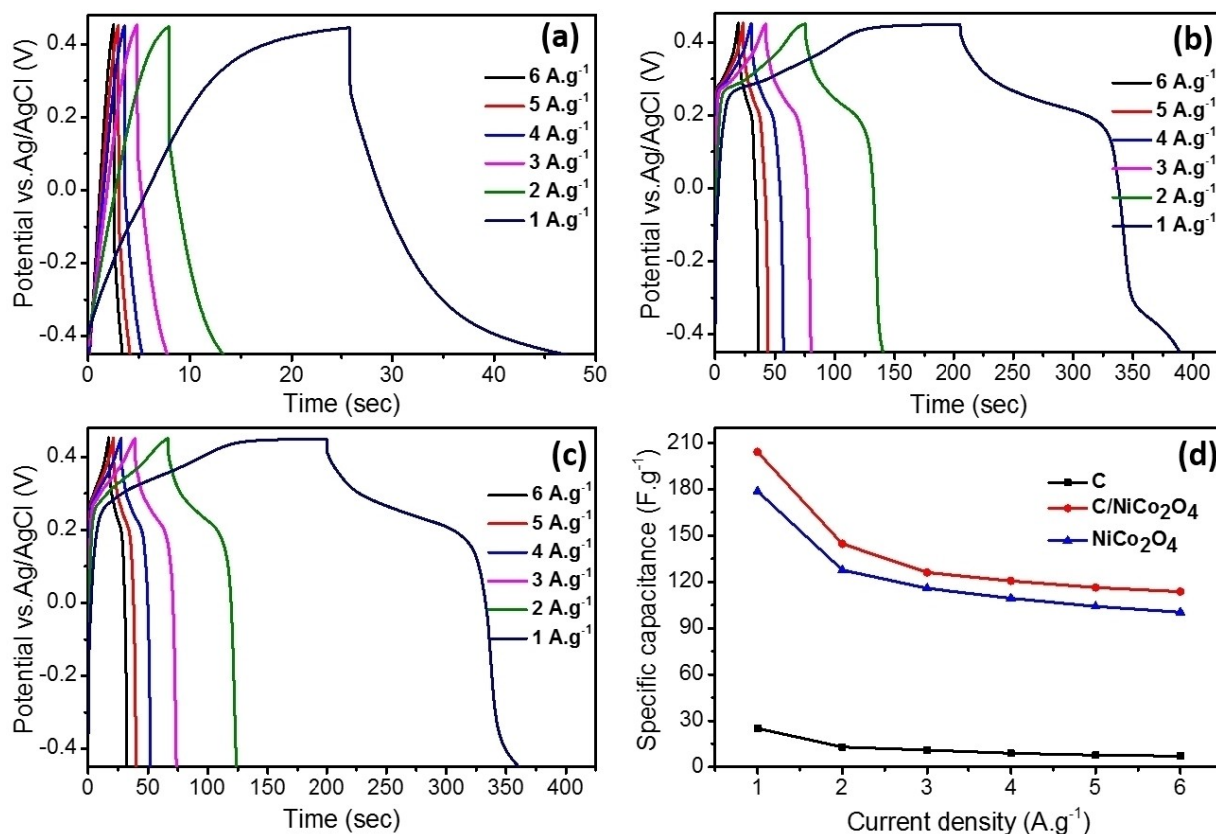
ChemistrySelect

Full Papers
doi.org/10.1002/slct.202001410

Chemistry Europe
European Chemical
Societies Publishing

Figure 5. (**a - c**) GCD curves, (**d**) Specific capacitance of the carbon, C/NiCo$_2$O$_4$ and NiCo$_2$O$_4$ at different current densities.

than those of pristine carbon and NiCo$_2$O$_4$: at a current density of 1 A.g^{-1}, C$_s$ of C/NiCo$_2$O$_4$ is 204.28 F.g^{-1}, which is higher than C$_s$ of NiCo$_2$O$_4$ (178.78 F.g^{-1}) and carbon (25.06 F.g^{-1}). These results agree well with the results of the CV analysis and show strong evidence of the synergistic effect between carbon and NiCo$_2$O$_4$ in C/NiCo$_2$O$_4$ material. This synergistic effect actually is the combination of both two charging mechanism in EDCL and PCs, which also appeared in composite materials based carbon and oxide metals such as: rGO@NiCo$_2$O$_4$,[17] rGO@NiCo$_2$O$_4$ on nickel foam,[18] 3D-Graphen@NiCo$_2$O$_4$,[29] NiCo$_2$O$_4$ on ultra-thin foam carbon 3D.[30] The Cs of C/NiCo$_2$O$_4$ composite is superior or equivalent to that of carbon, NiCo$_2$O$_4$ and their hybrid composites, as listed in Table 1.

The energy density (E) and power density (P) of the materials were calculated from the C$_s$ values at different current densities, and the results are plotted in Figure 6a. The energy density and power density of the C/NiCo$_2$O$_4$ are superior to pristine NiCo$_2$O$_4$ and carbon. The C/NiCo$_2$O$_4$ material delivers an energy density of 5.75 Wh.kg^{-1} at a power density of 112.5 W.kg^1. Even at high power density of 675 W.kg^{-1}, C/NiCo$_2$O$_4$ still delivers an energy density of 3.2 Wh.kg^{-1}. Meanwhile, energy density of carbon and NiCo$_2$O$_4$ is lower than that of C/NiCo$_2$O$_4$ at the same power density.

Table 1. Comparison of capacitance performance of previously reported carbon, NiCo$_2$O$_4$ and hybrid composite materials.

Electrode materials	Method of synthesis	Electrolyte	Window potential	C$_s$	Reference
NiCo$_2$O$_4$-decorated porous carbon	Hydrothermal/ Calcination	6 M KOH	0 – 0.5 V	596.8 F.g^{-1} at 2 A.g^{-1}	[16]
NiCo$_2$O$_4$-decorated carbon fiber	Solvothermal/ Calcination	2 M KOH	0 – 0.45 V	456 F.g^{-1} at 2 A.g^{-1}	[31]
NiCo$_2$O$_4$/Carbon active composite	Hydrothermal	6 M KOH	0 – 0.5 V	96.6 F.g^{-1} at 1 A.g^{-1}	[32]
Carbon-Based Spinel NiCo$_2$O$_4$	Hydrothermal	6 M KOH	0 – 0.6 V	201 F.g^{-1} at 2 A.g^{-1}	[33]
C/NiCo$_2$O$_4$	Hydrothermal/ Calcination	3 M KOH	-0.45 – 0.45	204.3 F.g^{-1} at 1 A.g^{-1}	This study

ChemistrySelect

Full Papers
doi.org/10.1002/slct.202001410

**Chemistry
Europe**

European Chemical
Societies Publishing
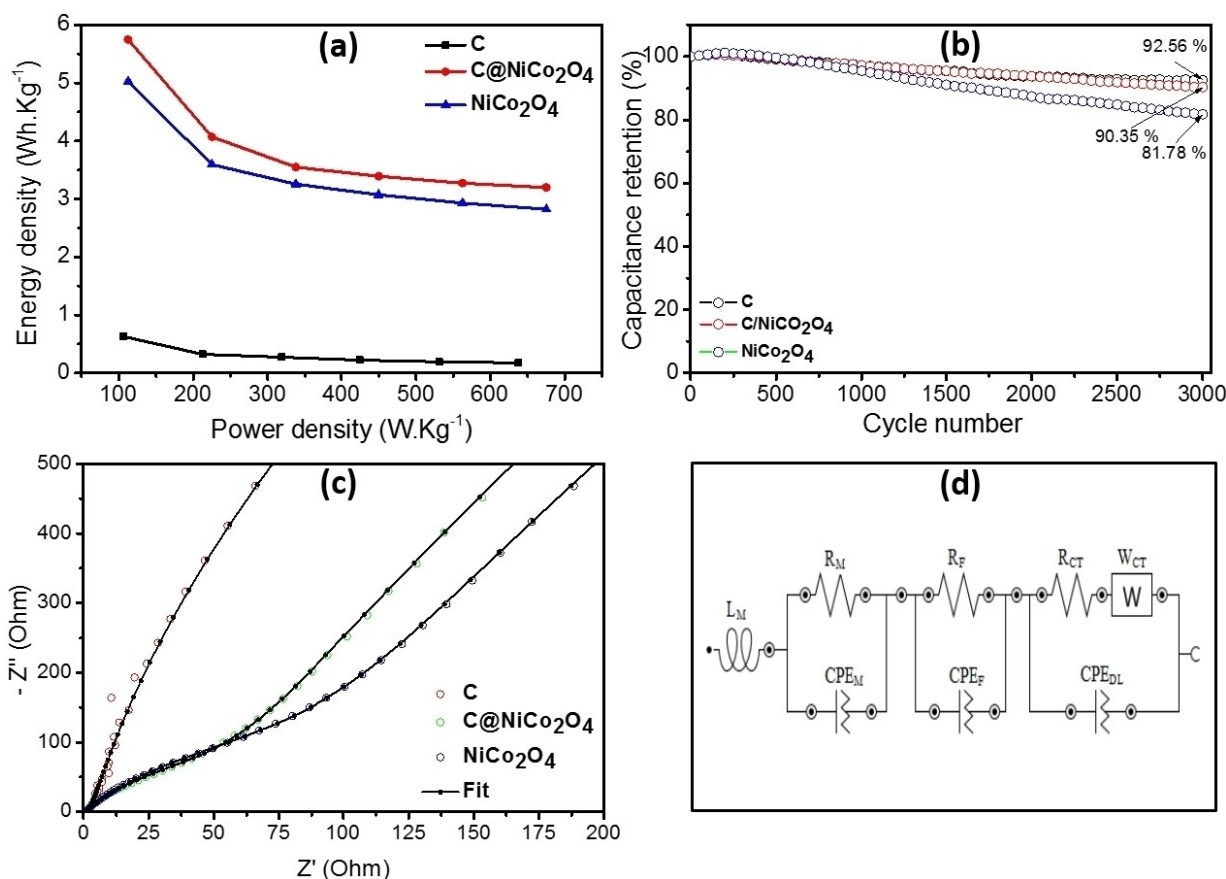
Figure 6. (a) Ragone plot of Carbon, $NiCo_2O_4$ and $C/NiCo_2O_4$; (b) Cycling performance of carbon, $NiCo_2O_4$ and $C/NiCo_2O_4$ for 3000 cycles at a current density of 2 $A.g^{-1}$; (c) Nyquist plots of carbon, $NiCo_2O_4$ and $C/NiCo_2O_4$ at full frequency range; (d) Equivalent circuit diagram used for fitting EIS data

Cycling stability

The cycling performance of synthesized materials was evaluated by repeating GCD measurement for 3000 cycles at a current density of 2 $A.g^{-1}$. For $NiCo_2O_4$ and $C/NiCo_2O_4$ materials, it can be seen that the C_s increases upon cycling and reaches the maximum at *ca.* 150th cycle (Figure 6b), meanwhile, C_s of carbon reaches maximum value on the first cycle. The maximum C_s of $NiCo_2O_4$ and $C/NiCo_2O_4$ corresponds to full activation of the $NiCo_2O_4$. As shown in Figure 6b, after 3000 cycles the C_s of carbon, $C/NiCo_2O_4$ and $NiCo_2O_4$ retained 92.56, 90.35 and 81.78%, respectively. The higher capacitance retention of $C/NiCo_2O_4$ compared to $NiCo_2O_4$ indicates the presence of carbon indeed contributed an important role. The carbon not only increases the electric storage capacity but also increases the stability of $NiCo_2O_4$ structure during faradaic charging/discharging reaction. The electrochemical performance of $C/NiCo_2O_4$ material clearly demonstrates that it is an attractive material for supercapacitor applications.

EIS analysis

To evaluated parameters related to the electrochemical reaction kinetics, EIS analysis was conducted in frequency range of

0.1 - 10^5 Hz and the Nyquist plots presented in Figure 6c. In order to understand the electrochemical behavior of the supercapacitors, an equivalent circuit was used to fit the Nyquist plots. As seen in Figure 6d, three components in the equivalent circuit can be respectively assigned to electrochemical responses of the electrode materials - including grain and interior grain boundary ((L_M-(R_M//CPE_M), electrode/electrolyte interphase ((R_{CT}-W_{CT})//CPE_{DL}), and pseudocapacitance contribution (R_F//CPE_F).[34] The fitted results were summarized in Table 2.

Generally, the impedance behaviors of the electrode/electrolyte interphases are quite similar, with the conductivity mostly depend on the Warburg diffusion processes. The characteristics of high conductivity and poor crystal structure of the synthetic carbon was respectively proved by a low value of R_M and a high value of CPE_M for the case of the carbon electrode. The fitted results were also pointed out the good pseudocapacitance behaviour of $NiCo_2O_4$ in comparison with the synthetic carbon material. As seen in the table, the Faradaic resistance (R_F) of the $NiCo_2O_4$ electrode (37.66 Ω) was much lower than that of the carbon electrode (2124.3 Ω). In summary, it can be concluded that the complementary contributions of the high conductivity of the hard carbon and

ChemistrySelect

Full Papers
doi.org/10.1002/slct.202001410

**Chemistry
Europe**
European Chemical
Societies Publishing

Table 2. Fitted parameters of equivalent circuit for EIS data of the Carbon, C/NiCo$_2$O$_4$ and NiCo$_2$O$_4$ electrodes.

Contributors /Activities	Parameters	Samples		
		C	C/NiCo$_2$O$_4$	NiCo$_2$O$_4$
Electrode material	L_M (H)	7.147E-16	4.6173E-6	1.5477E-7
	R_M (Ω)	38.869	39.515	89.37
	CPE_M (F)	0.032963	0.00889	0.003643
Faradaic capacitance	R_F (Ω)	2124.3	31.813	37.66
	CPE_F (F)	0.002683	0.00237	0.002963
	R_{CT} (Ω)	3.6587E-13	1.0924E-14	2.5993E-16
Electrode /electrolyte interphase	ZW_{CT} (Ω)	1871.6	1797.9	1312.1
	CPE_{DL} (F)	0.001049	0.00199	0.001887

the good pseudocapacitance behaviour of NiCo$_2$O$_4$ resulted in a superior performance of the C/NiCo$_2$O$_4$ supercapacitor.

3. Conclusions

The C/NiCo$_2$O$_4$ composite material has successfully prepared by facile combined hydrothermal treatment/calcination route. The XRD, TGA, FT-IR, Raman, SEM, TEM, EDS results confirmed the amorphous structure of carbon and the spinel structure of the as-prepared NiCo$_2$O$_4$ nanoparticles. The measurements of CV, GCD, and EIS revealed that the combination of carbon and NiCo$_2$O$_4$ created a synergistic effect, leading to higher C$_s$ of C/NiCo$_2$O$_4$ than that of pristine NiCo$_2$O$_4$ or carbon. The C/NiCo$_2$O$_4$ composite exhibited an excellent C$_s$ of 204.28 F.g^{-1} at a current density of 1 A.g^{-1}, meanwhile the C$_s$ of carbon and NiCo$_2$O$_4$ are 25.06 F.g^{-1} and 178.78 F.g^{-1}, respectively. The C/NiCo$_2$O$_4$ possessed high capacitance retention of 90.35% after 3000 cycles charge/discharge at a current density of 2 A.g^{-1}. In addition, the synthesized method was simple and low cost, which provided a feasible route for the mass-production of the porous metal oxides and amorphous carbon composite as supercapacitor materials.

Supporting Information Summary

Details of chemicals, material synthesis method, method of analyzing characterization and electrochemical for all synthesized materials are provided in supporting information.

Acknowledgments

Conflict of Interest

The authors declare no conflict of interest.

[1] A. S. Aricò, P. Bruce, B. Scrosati, J. M. Tarascon, W. Van Schalkwijk, *Nat. Mater.* **2010**, *4*, 148–159.
[2] a) Y. Guo, L. Yu, C. Y. Wang, Z. Lin, X. Wen David Lou, *Adv. Funct. Mater.* **2015**, *25*, 5184–5189; b) J. Zhao, C. Jiale, S. Xu, M. Shao, Q. Zhang, F. Wei, J. Ma, M. Wei, D. G. Evans, X. Duan, *Adv. Funct. Mater.* **2014**, *24*, 2938–2946; c) J. M. Tarascon, M. Armand, *Nature* **2001**, *414*, 359–367.
[3] Z. Salele Iro, *Int. J. Electrochem. Sci.* **2016**, *11*, 10628–10643.
[4] Y. J. Lee, H. W. Park, U. G. Hong, I. K. Song, *Curr. Appl. Phys.* **2012**, *12*, 1074–1080.
[5] H. Park, J. Seo, M. Kim, S.-H. Baeck, S. E. Shim, *Synth. Met.* **2015**, *199*, 121–127.
[6] C. Du, N. Pan, *Nanotechnology Law & Business* **2007**, *4*, 569–576.
[7] Y. B. Tan, J.-M. Lee, *J. Mater. Chem. A.* **2013**, *1*, 14814–14843.
[8] a) K.-y. Liu, Y. Zhang, W. Zhang, H. Zheng, G. Su, *Trans. Nonferrous Met. Soc. China* **2007**, *17*, 649–653; b) Z. Wu, Y. Zhu, X. Ji, *J. Mater. Chem. A.* **2014**, *2*, 14759–14772; c) Y. Li, X. Han, T. Yi, Y. He, X. Li, *J. Energy Chem.* **2019**, *31*, 54–78; d) P. Sun, N. Li, C. Wang, J. Yin, G. Zhao, P. Hou, X. Xu, *J. Power Sources* **2019**, *427*, 56–61; e) V.-N. Nguyen, T. Le, V. Thuy, V. Thao, M. Hatsukano, K. Higashimine, S. Maenosono, S. Chun, T. V. Thu, *Dalton Trans.* **2020**, *49*, 6718–6729.
[9] a) G. Qu, C. Li, P. Hou, G. Zhao, X. Wang, X. Zhang, X. Xu, *Nanoscale* **2020**, *12*, 4686–4694; b) T. V. Thu, V.-N. Nguyen, *J. Alloys Compd.* **2020**, *831*, 154921; c) G. Xiang, Y. Meng, G. Qu, J. Yin, B. Teng, Q. Wei, X. Xu, *Sci. Bull.* **2020**, *65*, 443–451.
[10] a) K. S. Ryu, Y.-G. Lee, Y.-S. Hong, Y. J. Park, X. Wu, K. M. Kim, M. G. Kang, N.-G. Park, S. H. Chang, *Electrochim. Acta* **2004**, *50*, 843–847; b) S. Bose, N. H. Kim, T. Kuila, K. t Lau, J. Lee, *Nanotechnology* **2011**, *22*, 295202; c) A. Eftekhari, L. Li, Y. Yang, *J. Power Sources* **2017**, *347*, 86–107.
[11] X.-C. Dong, Z. Yufei, L. Laiquan, H. Su, H. Wei, *J. Mater. Chem. A.* **2014**, *3*, 43–59.
[12] R. Alcántara, M. Jaraba, P. Lavela, J. Tirado, *Chem. Mater.* **2002**, *14*, 2847–2848.
[13] a) W. Cen, Y. Zhou, M. Ge, X. Xu, Z. Zhang, J. Z. Jiang, *J. Am. Chem. Soc.* **2009**, *132*, 46–47; b) Y. Yu, C. H. Chen, Y. Shi, *Adv. Mater.* **2009**, *19*, 993–997.
[14] a) M. Y. Ho, P. Khiew, D. Isa, T. K. Tan, W. S. Chiu, C.-h. Chia, *NANO* **2014**, *9*, 1430002; b) M. Zhi, C. Xiang, J. Li, M. Li, N. Wu, *Nanoscale* **2013**, *5*, 72–88; c) Z. Yi, L. P. Wang, M. T. Sougrati, Z. Feng, Y. Leconte, A. Fisher, M. Srinivasan, Z. Xu, *Adv. Energy Mater.* **2016**, 1601424-n/a.
[15] a) R. Dubey, V. Guruviah, *Ionics* **2019**, *25*, 1419–1445; b) A. Borenstein, O. Hanna, R. Attias, S. Luski, T. Brousse, D. Aurbach, *J. Mater. Chem. A.* **2017**, *5*, 12653–12672.
[16] V. Veeramani, R. Madhu, S.-M. Chen, M. Sivakumar, C.-T. Hung, N. Miyamoto, S.-B. Liu, *Electrochim. Acta* **2017**, *247*, 288–295.
[17] Y. Luo, H. Zhang, D. Guo, J. Ma, Q. Li, L. Chen, T. Wang, *Electrochim. Acta* **2014**, *132*, 332–337.
[18] C. Zhang, X. Geng, S. Tang, M. Deng, Y. Du, *J. Mater. Chem. A.* **2017**, *5*, 5912–5919.
[19] T. V. Thu, T. Van Nguyen, X. D. Le, T. S. Le, V. Van Thuy, T. Q. Huy, Q. D. Truong, *Electrochim. Acta* **2019**, *314*, 151–160.
[20] D. Li, Y. Gong, Y. Zhang, C. Luo, W. Li, Q. Fu, C. Pan, *Sci. Rep.* **2015**, *5*, 12903.
[21] J.-M. Syu, M.-L. Hsiao, C.-T. Lo, *J. Electrochem. Soc.* **2017**, *164*, A3903-A3913.

Chemistry
Europe
European Chemical
Societies Publishing

[22] A. Dychalska, P. Popielarski, W. Franków, K. Fabisiak, K. Paprocki, M. Szybowicz, *Mater. Sci. Pol.* **2015**, *33(4)*, 799–805.

[23] A. Mondal, S. Maiti, S. Mahanty, A. Panda, *J. Mater. Chem. A.* **2017**, *5*, 16854–16864.

[24] B. Wang, Y. Cao, Y. Chen, X. Lai, J. Peng, J. Tu, X. Li, *Nanotechnology* **2017**, *28*, 025501.

[25] Y. Gong, D. Li, Q. Fu, C. Pan, *Prog. Nat. Sci.*, 379–385.

[26] H. Wang, Q. Gao, L. Jiang, *Small* **2011**, *7*, 2454–2459.

[27] a) A. González, E. Goikolea, J. A. Barrena, R. Mysyk, *Renewable Sustainable Energy Rev.* **2016**, *58*, 1189–1206; b) Poonam, K. Sharma, A. Arora, S. K. Tripathi, *J. Energy Storage* **2019**, *21*, 801–825.

[28] J. Ren, W. Bai, G. Guan, Y. Zhang, H. Peng, *Adv. Mater.* **2013**, *25, 5965– 5970*.

[29] V. H. Nguyen, C. Lamiel, J.-J. Shim, *Mater. Lett.* **2016**, *170*, 105–109.

[30] J. Du, G. Zhou, H. Zhang, C. Cheng, J. Ma, W. Wei, L. Chen, T. Wang, *ACS Appl. Mater. Interfaces* **2013**, *5*, 7405–7409.

[31] J. Sun, W. Wang, D. Yu, *J. Electron. Mater.* **2019**, *48*, 1–11.

[32] J. Xu, F. Liu, X. Peng, J. Li, Y. Yang, D. Jin, H. Jin, X. Wang, B. Hong, *ChemistrySelect* **2017**, *2*, 5189–5195.

[33] M. Shahraki, S. Elyasi, H. Heydari, N. Dalir, *J. Electron. Mater.* **2017**, *46*.

[34] W. Wang, S. Guo, I. Lee, K. Ahmed, J. Zhong, Z. Favors, F. Zaera, M. Ozkan, C. Ozkan, *Sci. Rep.* **2014**, *4*, 4452.